Technical Note

Investigating interplay effects in pencil beam scanning proton therapy with a 4D XCAT phantom within the RayStation treatment planning system

den Boer, Erik; Wulff, Jörg; Mäder, Ulf; Engwall, Erik; Bäumer, Christian; Perko, Zoltan; Timmermann, Beate

DOI
10.1002/mp.14709

Publication date
2021

Document Version
Final published version

Published in
Medical Physics

Technical Note: Investigating interplay effects in pencil beam scanning proton therapy with a 4D XCAT phantom within the RayStation treatment planning system

Erik den Boer[†]
West German Proton Therapy Center Essen (WPE), Essen, Germany
Technical University Delft, Delft, Netherlands

Jörg Wulff[a)]
West German Proton Therapy Center Essen (WPE), Essen, Germany
University Hospital Essen, Essen, Germany
West German Cancer Center (WTZ), Essen, Germany
Institute of Medical Physics and Radiation Protection (IMPS), Technical University Mittelhessen, Gießen, Germany

Ulf Mäder
Institute of Medical Physics and Radiation Protection (IMPS), Technical University Mittelhessen, Gießen, Germany

Erik Engwall
RaySearch Laboratories, Stockholm, Sweden

Christian Bäumer
West German Proton Therapy Center Essen (WPE), Essen, Germany
University Hospital Essen, Essen, Germany
West German Cancer Center (WTZ), Essen, Germany
German Cancer Consortium (DKTK), Heidelberg, Germany
TU Dortmund University, Dortmund, Germany

Zoltan Perko
Technical University Delft, Delft, Netherlands

Beate Timmermann
West German Proton Therapy Center Essen (WPE), Essen, Germany
University Hospital Essen, Essen, Germany
West German Cancer Center (WTZ), Essen, Germany
German Cancer Consortium (DKTK), Heidelberg, Germany
Department of Particle Therapy, Essen, Germany

(Received 2 August 2020; revised 27 December 2020; accepted for publication 30 December 2020; published xx xxxx xxxx)

Purpose: Pencil beam scanning (PBS) for moving targets is known to be impacted by interplay effects. Four-dimensional computed tomography (4DCT)-based motion evaluation is crucial for understanding interplay and developing mitigation strategies. Availability of high-quality 4DCTs with variable breathing traces is limited. Purpose of this work is the development of a framework for interplay analysis using 4D-XCAT phantoms in conjunction with time-resolved irradiation patterns in a commercial treatment planning system (TPS). Four-dimensional dynamically accumulated dose distributions (4DDDs) are simulated in an in-silico study for a PBS liver treatment.

Methods: An XCAT phantom with 50 phases, varying linearly in amplitude each by 1 mm, was combined with the RayStation TPS (7.99.10). Deformable registration was used with time-resolved dose calculation, mapping XCAT phases to motion signals. To illustrate the applicability of the method a two-field liver irradiation plan was used. A variety $\sin^4$ type motion signals, varying in amplitude (1–20 mm), period (1.6–5.2 s) and phase (0–2π) were applied. Either single variable variations or random combinations were selected. The interplay effect within a clinical target (5 cm diameter) was characterized in terms of homogeneity index (HI5), with and without five paintings. In total 2092 scenarios were analyzed within RayStation.

Results: A framework is presented for interplay research, allowing for flexibility in determining motion management techniques, increasing reproducibility, and enabling comparisons of different methods. A case study showed the interplay effect was correlated with amplitude and strongly affected by the starting phase, leading to large variance. The average of all scenarios (single fraction) resulted in HI5 of 0.31 (±0.11), while introduction of five times layered repainting reduced this to 0.11(±0.03).

Conclusion: The developed framework, which uses the XCAT phantom and RayStation, allows detailed analysis of motion in context of PBS with comparable results to clinical cases. Flexibility in

defining motion patterns for detailed anatomies in combination with time-resolved dose calculation, facilitates investigation of optimal treatment and motion mitigation strategies. [https://doi.org/10.1002/mp.14709]

Key words: interplay effect, moving target, proton therapy, XCAT phantom

1. INTRODUCTION

Pencil beam scanning (PBS) proton therapy (PT), especially when applied as intensity-modulated PT, is becoming widely available as it allows for highest conformity to the target while sparing organs-at-risk. However, implementing proton PBS for targets affected by respiratory motion remains challenging.[1] The well-known interplay effect,[2,3] caused by the interplay between target and beam motion, is one of the main reasons why — at least without further mitigation strategies — PBS has to be applied with caution for targets that undergo motion during irradiation. In order to understand, evaluate, and possibly mitigate the impact on planned dose distributions by the interplay effect and other uncertainties of moving targets, the use of four-dimensional computed tomography (4DCT) is crucial. However, the availability of 4DCTs with high quality for a large patient cohort and with variable respiratory motion for research on the interplay effect is currently somewhat limited.

Four-dimensional computed tomography image sets are the basis for the calculation of four-dimensional dynamically accumulated dose distributions (4DDDs). In the 4DDD details on the time dependence of the delivery are considered together with changes in anatomy due to respiratory motion. Apart from experimental analysis as, for example, by Lee et al.,[3] at time of writing 4DDD is only available in research versions of treatment planning systems (TPS).[4–6] One of the most elaborate approaches to investigate the interplay effect was introduced by the PSI group. Boye et al.[7] used the concept of 4DCT(MRI) in which motion vectors from 4D magnetic resonance imaging (MRI) are warped to a single phase CT dataset. With a large library of anatomies extracted from 4D MRI, various potential motions could be evaluated on generated 4DCTs.

A flexible, but realistic computer model of the human body for multimodality imaging research, denoted the *XCAT phantom*, was developed by Segars et al.[8] It was proposed by Lomax[9] to use such phantoms for the investigation of motion effects in PBS. The XCAT phantom is available in various sizes/ages even including pediatrics.[10] Koybasi et al.[11] used a modified XCAT phantom to investigate the impact of regular/irregular breathing on under-dosage in internal target volume (ITV)-based proton treatment planning. To the authors' knowledge, the XCAT phantom has, however, not yet been employed for the analysis of interplay effects in PBS. The advantage of the XCAT phantom is that it is free of any imaging artifact that may occur in a 4DCT.[12,13] Furthermore, it allows for unambiguous contouring of organs and is flexible in defining its size. Thus, the XCAT phantom can serve as a self-consistent testing ground for interplay research, which has been evaluated in the frame of the current study.

The XCAT phantom was implemented in a framework with a research version of the RayStation TPS (version 7.99.10) to enable 4DDD calculations for user-defined respiratory motion curves. This approach allows for detailed studies of the interplay effect, its dependence on different properties of respiratory motion and mitigation. The overall capabilities of the framework are demonstrated by the investigation of a liver target irradiated with PBS.

2. MATERIALS AND METHODS

Figure 1 provides an overview of the overall workflow which allows the use of an arbitrary motion trace to calculate the 4DDD in the TPS RayStation. Details are given in the subsequent sections.

2.A. The XCAT phantom and definition of breathing curves

The XCAT phantom is based on 4D-tagged MRI and high-resolution respiratory-gated 4DCT patient data to establish accurate models for cardiac and respiratory motion, respectively. Organ volumes were obtained from International Commission on Radiological Protection (ICRP) publication 89,[14] a wide range of body measurements was taken from the Visible Human anatomies library of the National Library of Medicine.[15] Three-dimensional polygonal surfaces were created from the anatomical structures and used as input for generating nonuniform rational B-splines (NURBS) surface structures for abdominal organs. The XCAT software enables to create a phantom database of a large range of ages (from newborn to adults), body sizes, body mass indexes (including very slim and very obese models), and breathing motion parameters for both genders.[10,16]

The generation of the XCAT phantoms allows for a defined breathing motion curve,[17,18] however, it was deemed more flexible to leave the actual definition of the motion curve to the TPS. Hence, phases were exported from the XCAT configuration tool for a single linearly increasing motion amplitude, defined as the diaphragm deflection in cranio-caudal direction. Fifty phases with 1 mm spacing were created from maximum exhale to inhale, that is, a total amplitude of 5 cm. The library with the 50 phases is stored within RayStation as a so called examination group, which is standard container for 4DCTs. Note, the 50 phases and total

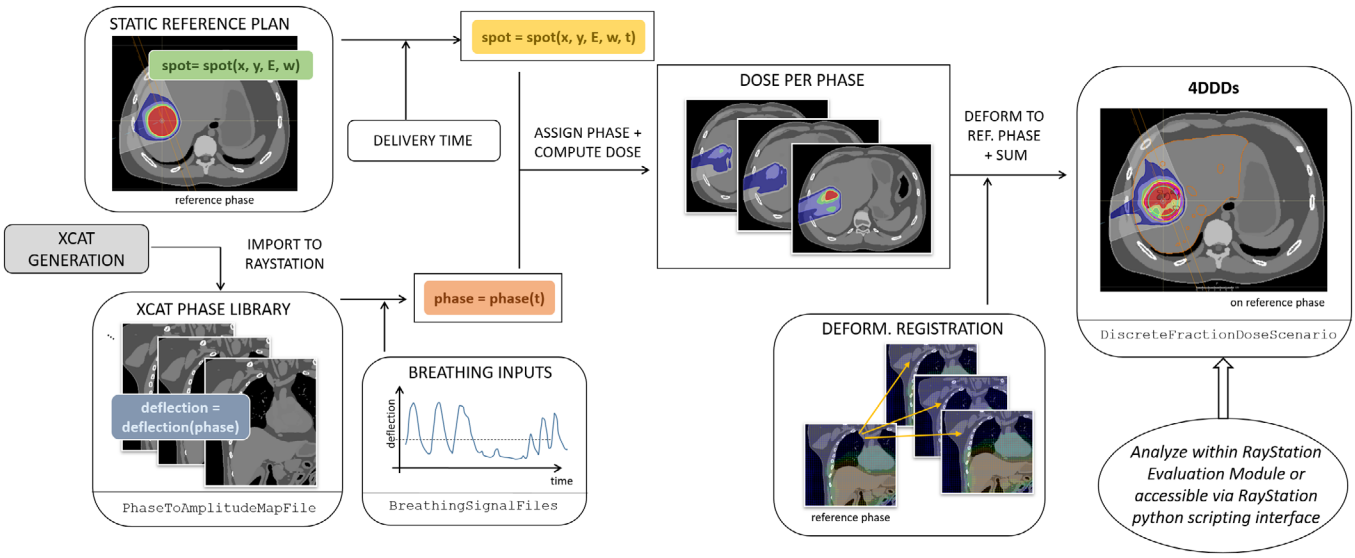

FIG. 1. Schematic overview of a 4DDD framework with the XCAT phantom in RayStation. Starting point is a plan in RayStation, calculated on a reference phase of the XCAT phantom. The interplay script calculates the 4DDD, based on the user supplied breathing input, phase-to-amplitude relation, parameters of the beam-time model and existing a deformable registration between all phases and the reference phase. The 4DDD is kept in RayStation as a separate dose scenario and can be analyzed subsequently. The import of the externally generated XCAT phases to build the phase library occurs only once. For details see Section 2.C.

amplitude of 5 cm were chosen to show the flexibility and resolution that can be achieved. A more tailored set to a specific investigation can be selected.

Two different versions of the phantom were generated. One contained realistic Hounsfield units (HU), while a second set served to label each organ with a unique intensity (see next section).

An individual motion trace as a function of time (Fig. 1) considered a relative movement of the diaphragm around the reference phase #26. The latter thus defined the mid position of the available ± 2.5 cm range.

2.B. Handling of the XCAT phantom in the treatment planning system RayStation

The 50 CTs were imported into the TPS RayStation as a 4DCT group. RayStation's Python-scripting interface was used to spatially register both phantom versions (see section above), define the contour of each organ by thresholding the unique intensity number and copying the contour to the version containing the realistic HU values.

The RayStation deformable image registration algorithm ANACONDA[19] was employed to internally construct the deformation vector fields from the reference phase to all other phases. Apart from the HU values, the organs in the direct vicinity (ribs, lung, liver, heart) of the diaphragm additionally served as "controlling regions of interest." The quality of the deformation was evaluated by computing the dice similarity coefficient for all phases. The original deformation fields of the XCAT phantom generation tool were not used with the chosen approach, which aimed at reflecting the clinical situation. Note that the deformation vector field could in principle be loaded to RayStation via a dedicated research interface.

2.C. 4DDD calculation in RayStation

The overall workflow is depicted in Fig. 1. The user starts with a plan created on one reference phase of the XCAT phantom. This plan can be created with any strategy that is offered in the TPS, for example, robustly optimized. A repainting scheme at field delivery can be accounted for by altering the original spot map to copy and reshuffle single spot locations and energy layers, respectively. This is achieved by accessing the internal spot-map representation via the RayStation scripting interface.[20] In this way volumetric or layered repainting can be considered.[4]

The actual interplay calculation is initialized from the RayStation application by calling a Python script `CreateInterplayScenarioGroup(..)`. The script defines the examination group, that is, the phase library, the delivery time parameters, a reference to breathing signal files and a phase to amplitude mapping, which will be explained in the following. A prerequisite for running the 4DDD is the existing deformable registration (see Section 2.B).

The temporal sequence of simulating pencil beams (or spots) considers the proton machine specific delivery behavior. The delivery time can be based on an empirical model, treatment log-files and a direct link to the IBA SCANALGO, which calculates the delivery sequence.[21] In the example calculations of the present work the time model of an IBA ProteusPlus system was employed which has been established and validated by Pfeiler et al.[5] This model considers the energy layer switching, dose rates and scan speeds.

The relation between a defined amplitude and the corresponding phase of the library is setup by means of a single look-up table in ASCII format (`PhaseToAmplitudeMapFile`). One or more breathing signals

(`BreathingSignalFiles`) in terms of amplitude vs time are defined within the main script as lists in ASCII format. With this implementation a phase can repeatedly be used, allowing for a flexible definition of motion curves, once the library and deformable registration (see Sections 2.A and 2.B) are established. Note, the amplitude in this implementation is basically just the link between the breathing signal and the phase, that is, it does not necessarily need to be the amplitude of the diaphragm used in this work.

After the individual pencil beam spots are assigned to the different phases, the dose per phase is calculated and afterwards mapped to the reference phase, taking the deformable image registration information into account. In a final step all phases are summed up, yielding the 4DDD, which is represented within RayStation as `DiscreteFractionDoseScenario`. Those scenarios are accessible from the evaluation module within RayStation, allowing an inspection of the resulting dose distribution. The script can be executed within a loop, thus calculating a large number of scenarios each defined by single breathing signal file in one common directory. The `DiscreteFractionDoseScenario` is accessible from within the RayStation scripting interface and thus quantitative metrics can easily be calculated for a large set of scenarios. A Python script was developed that, after the 4DDD calculation is finished, loops through all scenarios to calculate metrics as defined in Section 2.D.

The dose calculation in the 4DDD framework itself can be based on the RayStation Monte Carlo (MC) algorithm or the pencil beam algorithm (PBA). In this study the PBA was selected since the total number of scenarios was more than 2000. Even though the MC engine in RayStation is optimized for speed and accuracy for radiotherapy purposes, the total calculation time was too high with the available hardware. The main limitations of the PBA concern air cavities and sharp density gradients in the beam path. Neither was applicable for the investigated case, and therefore the reduction in accuracy was not considered significant.[22]

The interplay evaluations were considered as discrete scenarios within RayStation and quantitatively analyzed in terms of DVH metrics (see below).

2.D. Example case – liver target

To demonstrate the potential of the outlined framework, a liver treatment plan with a prescription dose of 4.2 GyRBE per fraction was analyzed. No averaging over treatment fractions was considered. A spherical clinical target volume (CTV) with 5 cm diameter was contoured in RayStation using the standard tools, positioned in the middle of the liver on the reference phase. An internal target volume was constructed by considering the phases 20–32, that is, a 12 mm motion range around the reference phase, leading to an ITV entirely within the liver. The ITV was created using the built-in RayStation tools for contour propagation, that is, deformation to selected phases and creating the encompassing union. A two-field single-field uniform dose (SFUD) plan was optimized with field-specific planning target volumes (PTV), accounting for 3.5% density uncertainty plus 2 mm range uncertainty, as well as 5 mm lateral margins.

A $\sin^4$ type of motion following

$$d(t) = \left(A_{ref} - \frac{A}{2}\right) + A \cdot sin^4\left(\frac{1}{T}(t-\theta)\right) \quad (1)$$

was employed to investigate the impact of the interplay effect on the treatment. In the above equation, $d(t)$ is the diaphragm deflection [mm] as a function of time t [s], A_{ref} is the deflection of the reference phase [mm] (see Section 2.A), A the modeled amplitude [mm], T is the period [s], and θ is the phase offset [rad]. Values for the amplitude of diaphragm motion and the period of one breathing cycle were modeled to be normally distributed with $A \sim N$ (12, 1.8) and $T \sim N$ (3.4, 0.17).[23,24] The start phase was uniformly distributed with $\sim\theta U$ (0,2π). All distributions were taken as uncorrelated, yielding a total of 1000 breathing motion curves. Additionally, three sets of calculations were performed with a single variable change only: the amplitude was changed between 1 and 20 mm in 1 mm steps (N = 20), while period and phase were kept constant at 3.4 s and 0 rad, respectively. Second, the period was varied between 1.6 and 5.2 s in steps of 0.3 s, with a constant amplitude of 12 mm and phase of 0 rad (N = 13). Lastly, the phase was altered between 0 and 2π rad in steps of 0.3 rad, with a constant amplitude of 12 mm and a period of 3.4 s (N = 13). Note that the same motion curve was always applied to both fields. The single breathing single files (see Section 2.C) were created in MATLAB R2019b.

The interplay effect was characterized in terms of the common homogeneity index HI5 for the CTV, defined as

$$HI5 = \frac{D_{5\%} - D_{95\%}}{D_{presc}} \quad (2)$$

with and without five times layered repainting, with D_x as highest dose delivered to x% of the CTV volume and prescribed dose D_{presc}.

3. RESULTS

The complete workflow allowed an efficient calculation of the 2092 interplay scenarios and analysis in the TPS RayStation. The computation of each scenario for the investigated treatment plan and the available 50 phases took between 12 and 15 min on the clinical hardware installation and a group of ~250 scenarios was executed as a single batch.

For the investigated liver case, controlling the registration with the liver, heart, lung, and ribs structures led to the best results. The dice similarity coefficient for the 49 XCAT phases calculated for the liver contour was 0.980 on average, with a minimum/maximum of 0.934 and 0.992, respectively. Other strategies in the deformable registration process, for example, only using the contoured structures of the XCAT phantom led to lower similarity values.

Figure 2 shows the relationship between the displacement of the diaphragm in cranio-caudal direction and the chest wall

of the XCAT phantom in anterior–posterior direction. The latter was determined as the average displacement vector for three points of interest on the phantom's chest wall, assessed by the deformable image registration. Within the span of investigated amplitudes between phases #36 and #16 a continuous, nearly linear relationship exists, also underlying the reasonable deformation vector field.

Figure 3 summarizes the homogeneity index HI5 for the CTV of the liver tumor test case. The results are given as a function of amplitude [Fig. 3(a)], period [Fig. 3(b)], and phase [Fig. 3(c)], either extracted from the complete set of randomly sampled breathing motion curves or based on changing the single variable only.

In total, more than 2000 data points were generated for the plans with and without repainting combined. The possibility to investigate so many cases allows for statistically significant conclusions to be drawn. Conversely, the set of results for signals with only a single variable shows the possibility to investigate specific elements of the overall problem of breathing in radiotherapy, even for ranges that are rare or unlikely in clinical practice, and thus difficult to find in patient databases.

With the possibility for evaluating a large number of scenarios, it is not only possible to carry out statistical analysis. The detection of general patterns also becomes more straightforward. A clear example can be seen in Fig. 3(c), which shows two clear peaks in the cloud of randomized results without repainting when considering only the starting phase offset. A possible explanation is that the most heavily weighted layers tend to be irradiated first and thus a major fraction of the overall dose may occur anatomy during the time interval of large anatomical changes. The effect is greatly suppressed for the repainting results. A next step would then be an investigation where gating is applied.

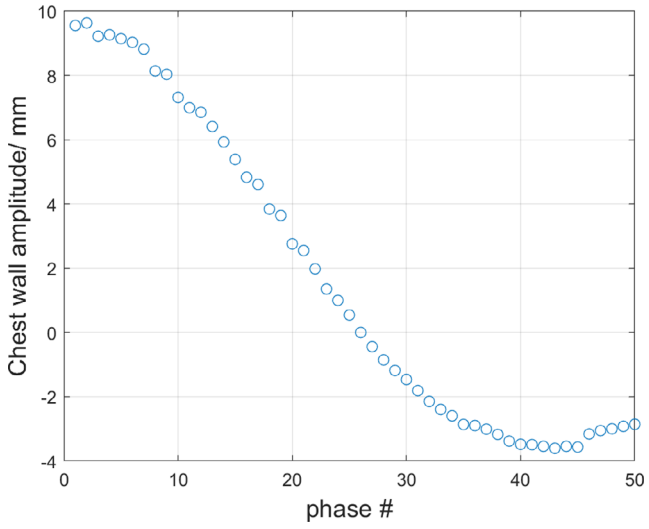

FIG. 2. Correlation between XCAT phantom chest wall and the amplitude that defines the XCAT phases. Such correlations enable conversion of external marker signals to tumor amplitude, allowing more flexibility when choosing the type of input signal and enabling comparison of results from work with different types of input signals.

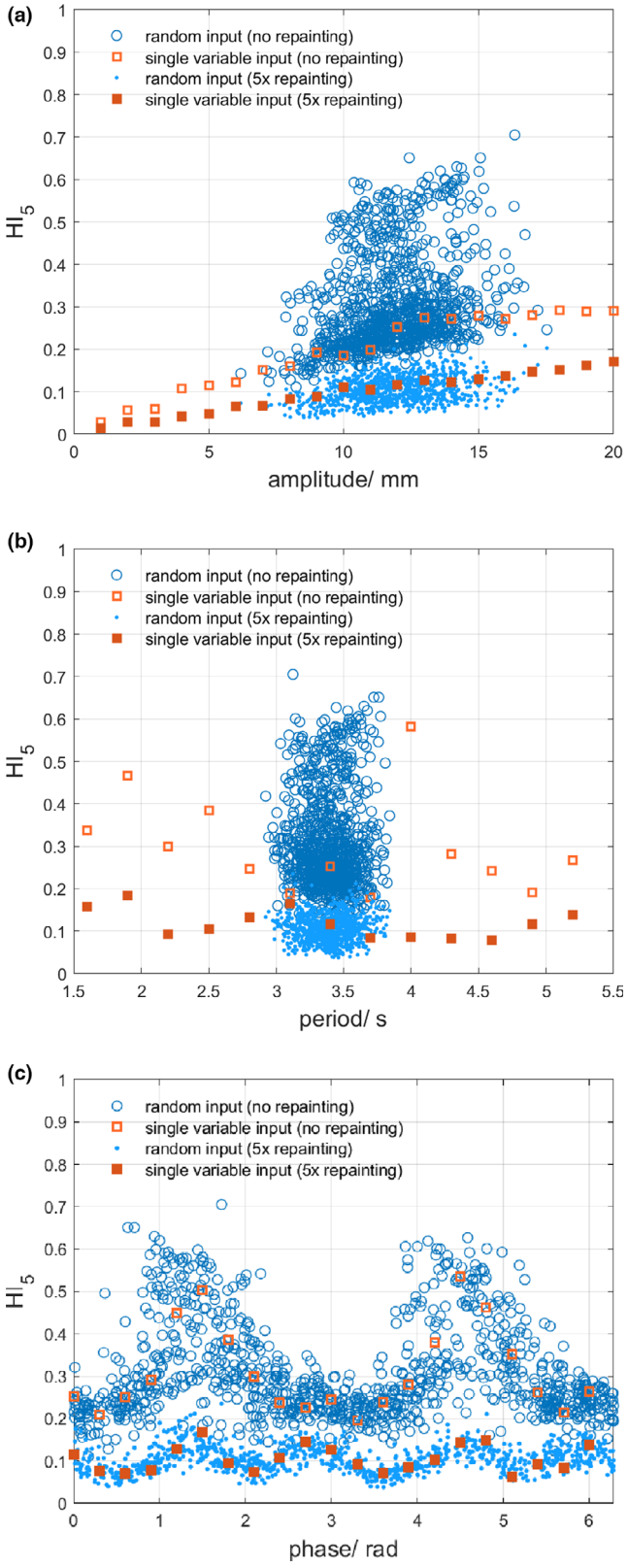

FIG. 3. Calculated homogeneity index (HI5) for the investigated breathing motion curves, with and without repainting, as a function of amplitude (a), period (b), and starting phase (c). The scenarios were either based on random sampling (circles) or single variable change only (squares). Note that the variable ranges of the randomized signals were based on Refs. [23,24], while the single variable analysis was done for an enlarged range, showing the flexibility of the framework.

4. DISCUSSION

The framework was used to efficiently calculate and evaluate 4DDD in the XCAT phantom with a spherical liver tumor.

The calculations show the expected results in terms of magnitude of the interplay effect. Although the investigated case is only limited to one plan and one target, the results can be compared with evaluation of clinical cases. In Pfeiler et al.[25] various liver targets with variable motion amplitudes were investigated. The 4DDD was calculated based on a clinical 4DCT and averaged over 60 different starting phases and layer-switching times. The HI5 for a tumor of comparable size and an amplitude of 5 mm was approximately 0.1 without the application of repainting. This fits in general to the trend in Fig. 3(a). Siregar et al.[22] used the same dataset and investigated the impact of repainting. Layered repainting (five times) led to a slight improvement of HI5 to 0.05, also agreeing in general with the findings here. Nevertheless, a more direct comparison with real patient CTs directly matching the anatomy of the XCAT phantom and the target in the liver could be performed, which is left for further studies.

The strong impact of phase was already demonstrated by Bert et al.[26] This effect will strongly depend on the delivery characteristics of the proton accelerator, plan details and tumor size. The dosimetric implications of varying all of those parameters can systematically be investigated with the developed framework. Furthermore, other clinical parameters of interest could be extracted from the resulting 4DDD, such as V_{95}, V_{107}, $D_{max,}$ and D_{min}.

It needs to be emphasized, that the input curves used here followed a simplistic $\sin^4$ type, although the framework itself works with an arbitrary shape of input signal. It is left for further studies to systematically analyze the impact of breathing irregularities.

As expected, repainting does not completely remove the interplay effect.[27] However, the variability in the results is significantly reduced. As the example only considered a single fraction, the fractionation effect of a typical treatment scheme will further reduce the dose deterioration by the interplay effect. The radiobiological consequences of inhomogeneous dose distribution in a single fraction is, however, not clear. One can expect that the fractionation will certainly be more effective if the variation of the results is kept small, that is, by applying layered repainting. The most appropriate way to tracking the impact of motion throughout the treatment course could be the approach of Meijers et al.[6] The corresponding investigation with different breathing curves per treatment fraction is in principle possible with the developed framework.

The developed methodology strongly depends on the accuracy of the XCAT phantom and the DIR within RayStation. It was recently discussed by Eiben et al.[28] that the XCAT phantom may produce inconsistent and noninvertible deformations. The tumor model in the present study was delineated within RayStation and then deformed, that is, relying on the invertible deformation of the ANACONDA algorithm.[19] It is also possible to create simple tumors suing the XCAT software, so that they are deformed as the phantom phases are rendered. Furthermore, the tumor was a simple sphere within the liver where no density changes or organ sliding occurs. Hence, the limitations described were considered not relevant in this study, but the proposed postprocessing by Eiben et al.[28] could generally be incorporated in the overall workflow. Furthermore, a lung mass conservation as developed by Williams et al.[29] was not considered in the used version of the XCAT phantom here. This extension may be of importance when exploring PBS lung treatments.

It should be noted that it is possible to pass a breathing curve as input to the XCAT phantom directly, yielding a 4DCT set that corresponds to the selected anatomy for the given breathing pattern. Varying period or starting phase is possible with this method, but any other changes, or combinations of variations, would require manual reshuffling. Creating the 4DCT sets for many breathing patterns is intensive both in time and in computational requirements. The same variation can be achieved using the approach described here, provided that the signal and XCAT are generated with sufficiently high resolution, at a fraction of the cost. However, using one phantom to investigate different amplitudes by selecting subsets of phases can impact the anatomical accuracy of specific breathing patterns. In this work, 50 phases were generated, and subsets used to show the flexibility and resolution that can be achieved, but such high resolution would only be necessary for special cases. When searching for more generally applicable clinical conclusions, it would be better to tailor the phantom to the breathing signals under consideration. Similarly, the difference between inhalation and exhalation — specifically a possible hysteresis — was not considered in this study. In principle, however, this can be modeled using the XCAT phantom.

The use of 50 phases has a direct impact on the calculation speed. If for instance only 10 ten are employed the total calculation time is reduced to only ~2 min per scenario. Although the underlying dose calculation itself is only depending on the total number of spots, the overall calculation is affected by the number of phases. This is caused by the required internal spot redistribution and the number of deformations at the end of the calculation (see Fig. 1). Hence, a more tailored set of phases may also be appropriate if computation times compromise the scope of an in-silico study.

A natural progression from the current work would be the incorporation of patient breathing data, such as gathered in Ref. [30]. This was not done in this work to allow for more control over the variation of parameters but limits its clinical applicability. Furthermore, care should be taken to make sure that the phantom is similar to the anatomy of the patient of whom breathing data are used. However, the choice of breathing signal is important in this case. The XCAT phantom uses diaphragm position to calculate its deformations, but many systems for breathing monitoring use a surrogate signal, such as chest wall deflection. Although the correlation of the (external) surrogate and tumor/diaphragm motion may vary from patient to patient and even fraction to fraction,[31] the XCAT phantom allows a convenient way to analyze, for example,

the impact of location of an external surrogate for an average patient.

The investigated case considered a single size/age phantom only. The investigation for different anatomies, for example, pediatric patients is left for future research. Given the flexibility of the described framework, this is considered straight forward. It should be stressed that the established XCAT models are specific of a class of cases but not patient specific.

5. CONCLUSION

A flexible framework for research on motion in proton therapy within the RayStation TPS was developed. The application to an example case of a liver tumor shows the expected dependence of the interplay effect on motion parameters. The XCAT phantom allows for the definition of arbitrary motion patterns and can be considered a realistic representation of the human body under motion. Given the flexibility of the methodology, this will help to further investigate of planning strategies to reduce the impact of motion in proton therapy are feasible. If other researchers in the community will also use a common dataset such as the XCAT phantom, results can be made more comparable.

ACKNOWLEDGMENTS

The authors thank Marcel Zuschlag for his help preparing the XCAT phantom and Tina Pfeiler for performing initial tests. Open Access funding enabled and organized by ProjektDEAL.

CONFLICT OF INTEREST

Erik Engwall is employee of RaySearch Laboratories, Sweden, Stockholm.

[†]Present address: Ion Beam Applications, Essen, Germany
[a)]Author to whom correspondence should be addressed. Electronic mail: joerg.wulff@uk-essen.de.

REFERENCES

1. Chang JY, Zhang X, Knopf A, et al. Consensus guidelines for implementing pencil-beam scanning proton therapy for thoracic malignancies on behalf of the PTCOG thoracic and lymphoma subcommittee. *Int J Radiat Oncol Biol Phys*. 2017;99:41–50.
2. Seco J, Robertson D, Trofimov A, Paganetti H. Breathing interplay effects during proton beam scanning: simulation and statistical analysis. *Phys Med Biol*. 2009;54:N283–N294.
3. Lee E, Perry D, Speth J, Zhang Y, Xiao Z. Measurement-based study on characterizing symmetric and asymmetric respiratory motion interplay effect on target dose distribution in the proton pencil beam scanning. *J Appl Clin Med Phys*. 2020;21:59–67.
4. Engwall E, Glimelius L, Hynning E. Effectiveness of different rescanning techniques for scanned proton radiotherapy in lung cancer patients. *Phys Med Biol*. 2018;63:095006.
5. Pfeiler T, Bäumer C, Engwall E, et al. Experimental validation of a 4D dose calculation routine for pencil beam scanning proton therapy. *Z Med Phys*. 2018;28:121–133.
6. Meijers A, Jakobi A, Stützer K, et al. Log file-based dose reconstruction and accumulation for 4D adaptive pencil beam scanned proton therapy in a clinical treatment planning system: implementation and proof-of-concept. *Med Phys*. 2019;46:1140–1149.
7. Boye D, Lomax T, Knopf A. Mapping motion from 4D-MRI to 3D-CT for use in 4D dose calculations: a technical feasibility study. *Med Phys*. 2013;40:061702.
8. Segars WP, Sturgeon G, Mendonca S, Grimes J, Tsuiet BMW. 4D XCAT phantom for multimodality imaging research. *Med Phys*. 2010;37:4902–4915.
9. Lomax A. What will the medical physics of proton therapy look like 10 yr from now? A personal view. *Med Phys*. 2018;45:e984–e993.
10. Segars WP, Norris H, Sturgeon GM, et al. The development of a population of 4D pediatric XCAT phantoms for imaging research and optimization. *Med Phys*. 2015;42:4719–4726.
11. Koybasi O, Mishra P, St James S, Lewis JH, Seco J. Simulation of dosimetric consequences of 4D-CT-based motion margin estimation for proton radiotherapy using patient tumor motion data. *Phys Med Biol*. 2014;59:853–867.
12. Sentker T, Schmidt V, Ozga A-K, et al. 4D CT image artifacts affect local control in SBRT of lung and liver metastases. *Radiother Oncol*. 2020;148:229–234.
13. Yamamoto T, Langner U, Loo BW, Shen J, Keall PJ. Retrospective analysis of artifacts in four-dimensional CT images of 50 abdominal and thoracic radiotherapy patients. *Int J Radiat Oncol Biol Phys*. 2008;72:1250–1258.
14. ICRP. *Basic Anatomical and Physiological Data for Use in Radiological Protection Reference Values*. ICRP Publication 89. Vol. Ann. ICRP 32 (3-4); 2002.
15. Medicine, T.N.L.o. The National Library of Medicine's Visible Human Project. Available from https://www.nlm.nih.gov/research/visible/visible_human.html
16. Segars WP, Mahesh M, Beck TJ, Frey EC, Tsui BMW. Realistic CT simulation using the 4D XCAT phantom. *Med Phys*. 2008;35:3800–3808.
17. Mishra P, St James S, Paul Segars W, Berbeco RI, Lewis JH Adaptation and applications of a realistic digital phantom based on patient lung tumor trajectories. *Phys Med Biol*. 2012;57:3597–3608.
18. Myronakis ME, Cai W, Dhou S, et al. A graphical user interface for XCAT phantom configuration, generation and processing. *Biomed Phys Eng Expr*. 2017;3:017003.
19. Weistrand O, Svensson S. The ANACONDA algorithm for deformable image registration in radiotherapy. *Med Phys*. 2015;42:40–53.
20. RaySearchLaboratories. *RAYSTATION 9B Scripting Guideline*. RaySearch Laboratories AB (publ); 2019. **5.3.027**.
21. Engwall E, Fredriksson A, Glimelius L. 4D robust optimization including uncertainties in time structures can reduce the interplay effect in proton pencil beam scanning radiation therapy. *Med Phys*. 2018;45:4020–4029.
22. Siregar H, Bäumer C, Blanck O, et al. Mitigation of motion effects in pencil-beam scanning - impact of repainting on 4D robustly optimized proton treatment plans for hepatocellular carcinoma. *Zeitschrift für Medizinische Physik*. 2020; in press.
23. Gierga DP, Chen GTY, Kung JH, Betke M, Lombardi J, Willett CG. Quantification of respiration-induced abdominal tumor motion and its impact on IMRT dose distributions. *Int J Radiat Oncol Biol Phys*. 2004;58:1584–1595.
24. Kirilova A, Lockwood G, Choi P, et al. Three-dimensional motion of liver tumors using cine-magnetic resonance imaging. *Int J Radiat Oncol Biol Phys*. 2008;71:1189–1195.
25. Pfeiler T, Khalil DA, Ayadi M, et al. Motion effects in proton treatments of hepatocellular carcinoma—4D robustly optimised pencil beam scanning plans versus double scattering plans. *Phys Med Biol*. 2018;63:235006.
26. Bert C, Grözinger SO, Rietzel E. Quantification of interplay effects of scanned particle beams and moving targets. *Phys Med Biol*. 2008;53:2253–2265.
27. Bernatowicz K, Lomax AJ, Knopf A. Comparative study of layered and volumetric rescanning for different scanning speeds of proton beam in liver patients. *Phys Med Biol*. 2013;58:7905–7920.
28. Eiben B, Bertholet J, Menten MJ, Nill S, Oelfke U, McClelland JR. Consistent and invertible deformation vector fields for a breathing

anthropomorphic phantom: a post-processing framework for the XCAT phantom. *Phys Med Biol*. 2020;65:165005.
29. Williams CL, Mishra P, Seco J, et al. A mass-conserving 4D XCAT phantom for dose calculation and accumulation. *Med Phys*. 2013;40:071728.
30. Ernst F. *Algorithms for Compensation of Quasi-periodic Motion in Robotic Radiosurgery*. New York, NY: Springer; 2011.
31. Trnková P, Knäusl B, Actis O, et al. Clinical implementations of 4D pencil beam scanned particle therapy: report on the 4D treatment planning workshop 2016 and 2017. *Physica Med*. 2018;54:121–130.